

## D. I3.2.1 Site specific report on geophysical survey on site

David Caterina, Itzel Isunza Manrique, Marc Dumont,  
Frédéric Nguyen  
*ULiège*  
Version 1.0



## SUMMARY

---

1	Introduction.....	2
1.1	Summary of the study area.....	2
1.1.1	Site history.....	2
1.1.2	Geology and hydrogeology.....	4
1.2	Summary of available ground truth data prior to the geophysical survey.....	5
2	Geophysical investigations.....	7
2.1	Geophysical methods and coverage.....	7
2.2	Geophysical processing and results.....	10
2.2.1	EMI results.....	10
2.2.2	MAG results.....	11
2.2.3	ERT and IP results.....	13
2.2.4	SRT – MASW results.....	16
3	Conclusion.....	18
4	References.....	19

# 1 INTRODUCTION

## 1.1 SUMMARY OF THE STUDY AREA

The following report describes the results of the geophysical survey that was carried out from September 28<sup>th</sup> to October 2<sup>nd</sup>, 2020 on the site of DUFERCO - La Louvière (Wallonia, Belgium). An aerial view of the site taken in 2020 is presented in Figure 1 together with different zones of interest for the NWE-REGENERATIS project. As part of the geophysical characterization, the investigations were mainly focused on the white slag and old factory areas (see green and orange polygons respectively).

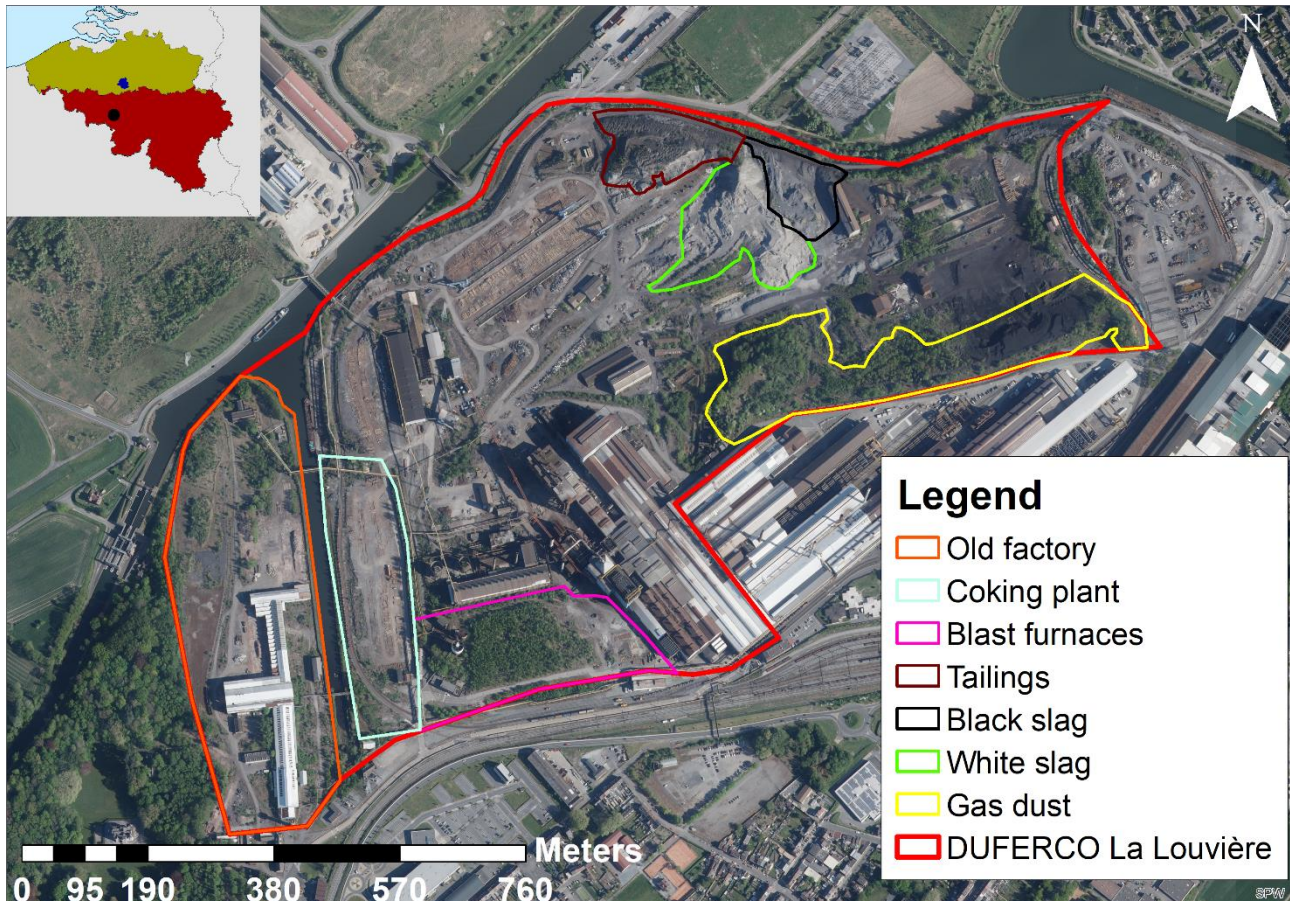
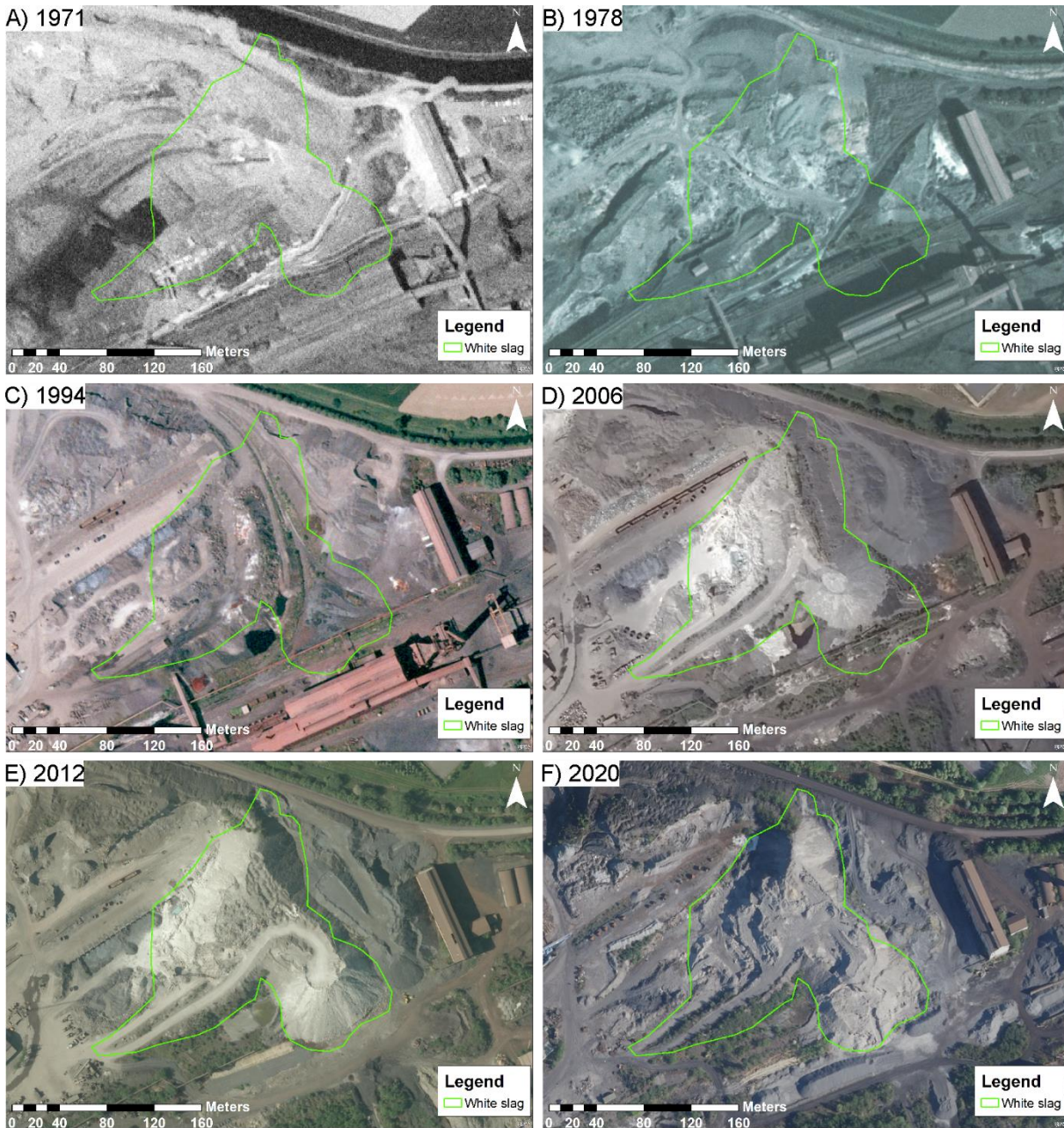


Figure 1 : Aerial view of the Dufenco - La Louvière site with the delimitation of several potentially interesting areas for NWE-REGENERATIS.

### 1.1.1 Site history

Detailed historical information about the “La Louvière” site can be found in the deliverable *DI3.1.1: Site specific report summarizing available historical data*. In the following, only a brief description of the surveyed areas will be presented.

Aerial photographs of the white slag heap taken at different times are presented in Figure 2. From these photographs, it appears clearly that the whole area was heavily modified over the years until recently. We can note that the white slag heap rise between 1994 and 2012, afterward deposits have been displaced or removed. The historical study indicates that the materials constituting the heap are mainly raw materials and by-products of the iron/steel-making activities (slag, coke, ores). Due to the shutdown of the deferrization unit in 2011, it is likely that the most recent layers of the slag heap contain a mixture of different materials (scrap metal, wood, aluminum ingots, slag, refractories, plastics).



*Figure 2 : Evolution of the white slag area over the years.*

Figure 3 shows the evolution of the old factory from 1971 to 2020. While most of the buildings in the area remain present until very recently, changes of soil occupation are observed in the western part. Dark material appears to have been deposited in piles (Figure 3B) and subsequently spread or removed (Figure 3C-E). Today, the whole area is flat, buildings in the east have been dismantled and vegetation has partially colonized the northern area (Figure 3F). Deposits of different colors/natures are still observed on the ground surface in the western part.

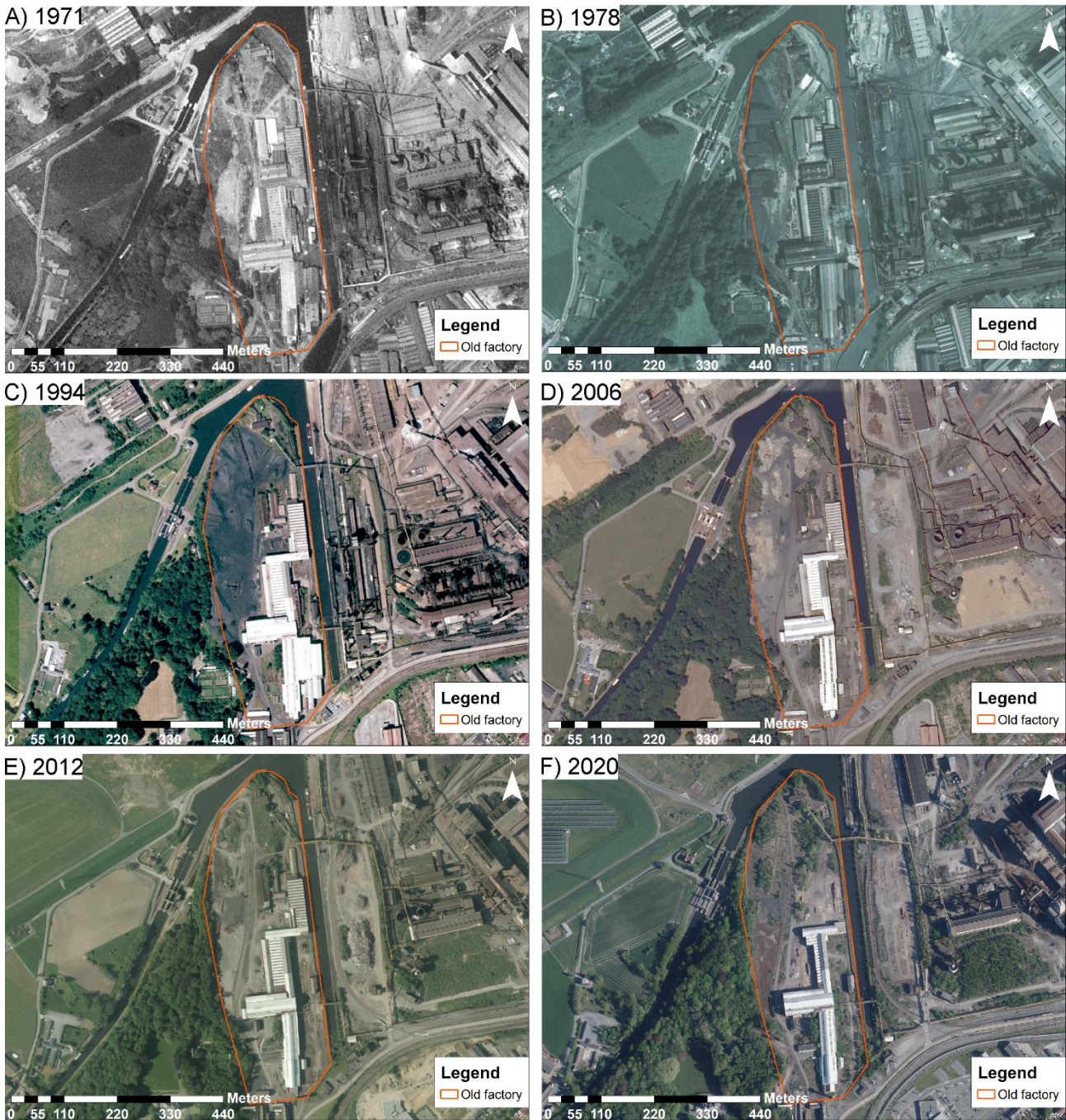


Figure 3 : Evolution of the old factory area over the years.

### 1.1.2 Geology and hydrogeology

The geological map presented in Figure 4 indicates that most of the white slag heap is underlain by alluvium from the Thiriau stream. These quaternary deposits, which can be up to 8 to 10 meters thick, are composed of alternating sandy and clayey layers with local gravel content. Parts of the slag heap may also lie on the Houiller formation made of shale, sandstone and coal.

Such geological formations are also present in the northern part of the old factory, while in its southern part, sandy and clayey sediments from the Hannut and Carnières formations are found. It is however important to mention that the whole site has been covered over time with backfill deposits that may reach a thickness of several meters and even tens of meters in some places.

From a hydrogeological point of view, perched water tables are expected in the backfill that covers the whole site. The hydrogeological properties of these deposits depend on the material of which

they are composed and exhibit likely heterogeneous patterns. Groundwater flows in these horizons are probably disturbed by the heterogeneity of the deposits and by the presence of deep foundations. A groundwater table in the alluvium of the Thiriau stream is also expected as well as a (deeper) groundwater table in the Houiller formation.

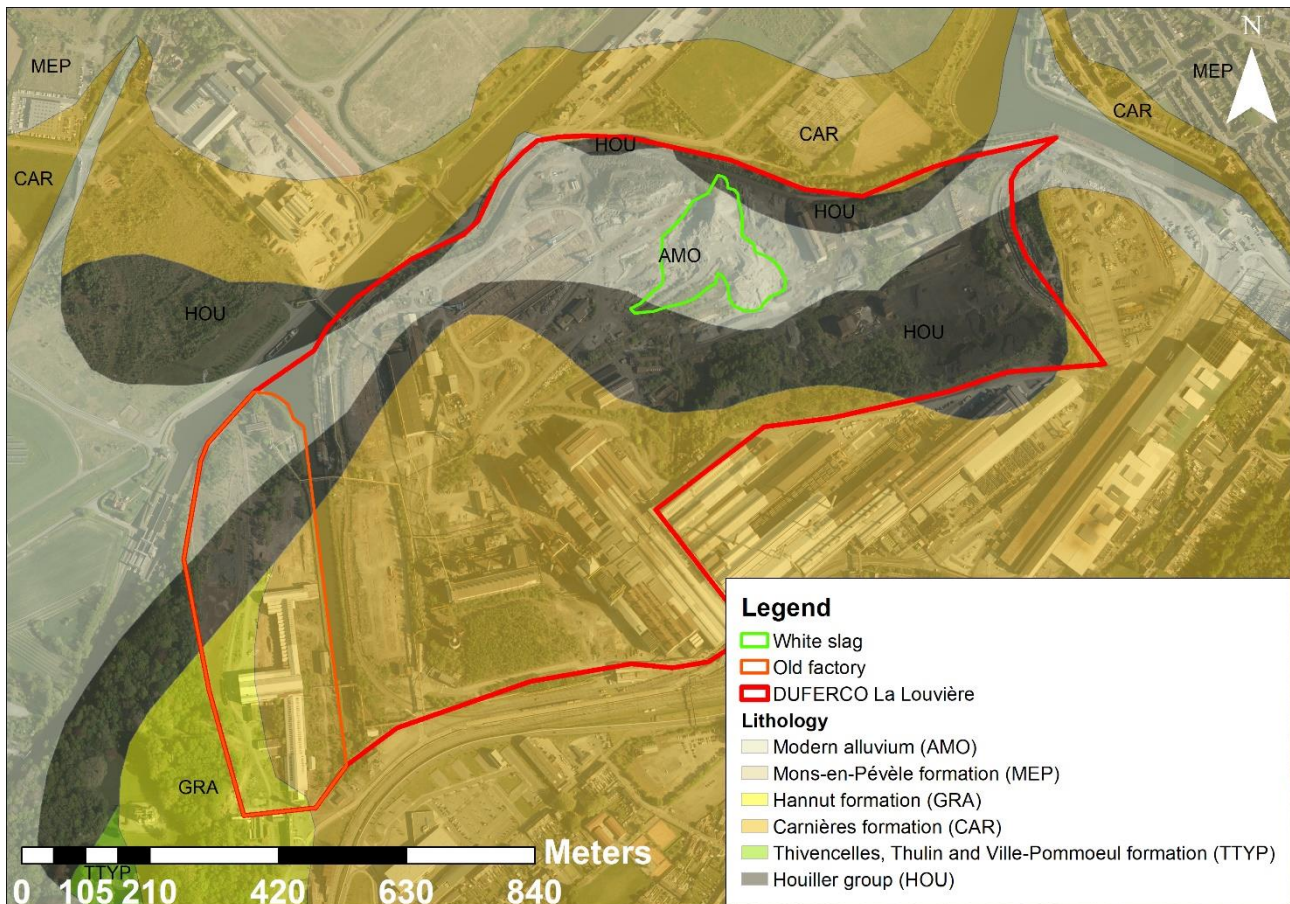


Figure 4 : Excerpt of the geological map of the site

## 1.2 SUMMARY OF AVAILABLE GROUND TRUTH DATA PRIOR TO THE GEOPHYSICAL SURVEY

In 2017, several trial pits were conducted in the white slag heap (see locations in **Erreur ! Source du renvoi introuvable.**). On this occasion, several samples were collected and analysed. Unfortunately, the results of the analyses performed are confidential and cannot be used in the project. Nevertheless, the photographs taken during the trial pitting already provide valuable information (see Figure 5).

The trial pits on top of the heap (P1 and P2) showed fine homogeneous material. In P3 and P4, the white slag appeared to be mixed with other materials such as refractory or construction waste. In the trench (PC) whose dimension were 15 m long, 10 m wide and 7 m deep, slag was again mixed with other materials (metal, wood, plastic...), the proportion of the white slag tending to decrease with depth. On the sides of the heap (FA, FB and FC), heterogeneity was still visible in the form of white slag mixed with all kinds of debris/materials.

Little information is available on the nature of the material deposited in the western area of the former factory.

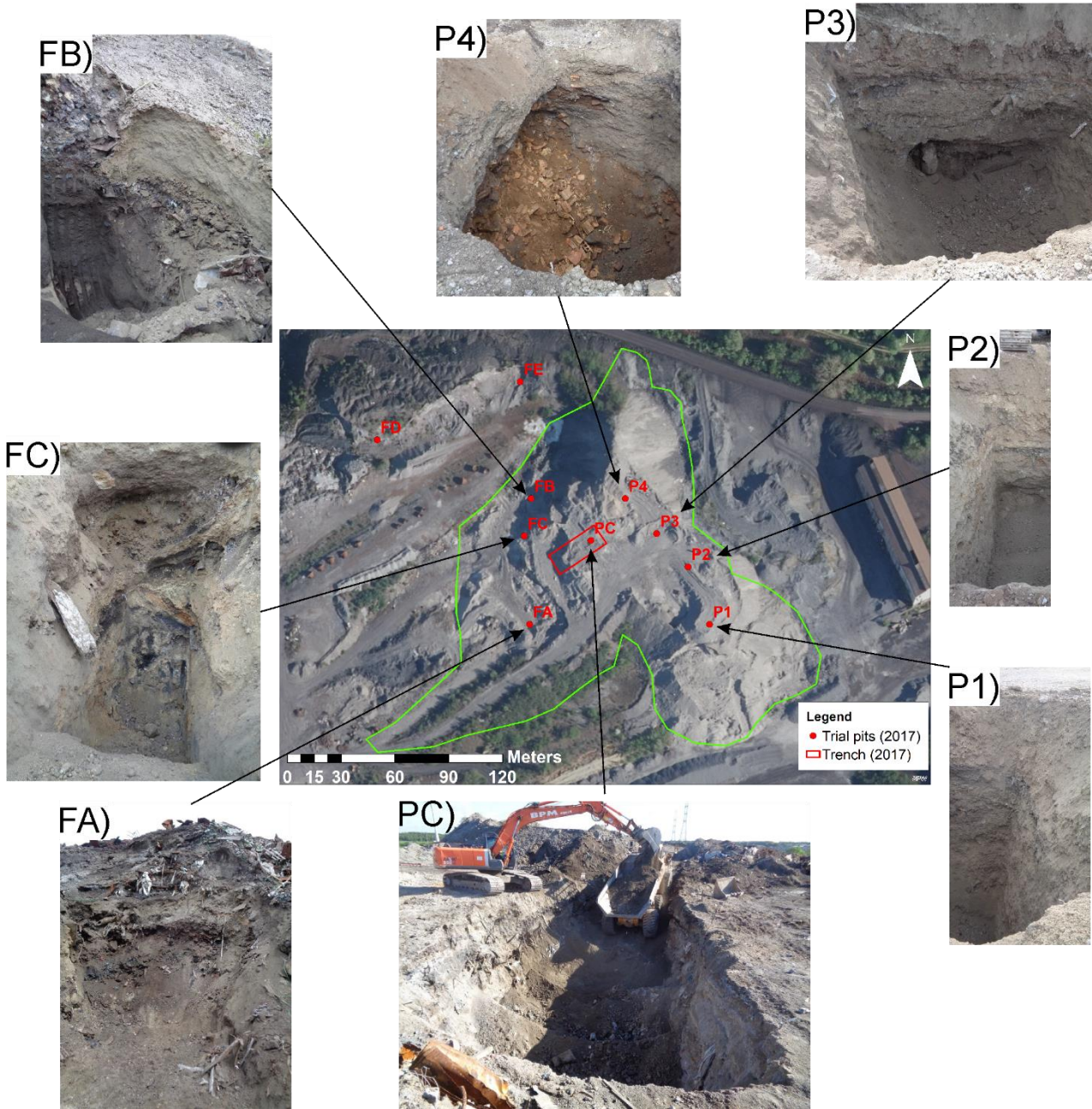


Figure 5 : Map of the trial pits and the trench carried out on the white slag heap (and surrounding) in 2017 (center of the figure) together with photographs taken during the trial pitting/trenching. P1 and P2 exhibit fine and homogeneous material, P3 shows white slag on top and refractory material at the bottom, P4 shows white slag on top and a heterogeneous waste at the bottom, PC is a large trench (15 m long, 10 m wide, 7 m deep) where slag is mixed with heterogeneous waste (metal, wood, plastic) whose proportion tends to decrease with depth, FA is composed of fine white slag mixed with waste, FB consists of white slag on top and dark material at the bottom, and FC is made of white slag mixed with mineral waste.

## 2 GEOPHYSICAL INVESTIGATIONS

ULiege team conducted two geophysical surveys on the Duferco - La Louvière site. The first took place in 2017 during NEW-RAWFILL project and was only focused on the white slag heap. It consisted of several Electrical Resistivity Tomography and Induced Polarization profiles. An overview of the results obtained is available in the deliverable *D.I3.1: Geophysical survey design of La Louvière (Duferco) site*. The second survey was conducted as part of the NWE-REGENERATIS project and took place from September 28<sup>th</sup> to October 2<sup>nd</sup>, 2020. Here below, the geophysical methods applied will first be briefly introduced and then the results presented.

### 2.1 GEOPHYSICAL METHODS AND COVERAGE

In the following, geophysical methods applied on the site are listed with emphasis on the target properties and their potential usefulness for characterizing past-metallurgical sites. Different geophysical methods allow to estimate several physical properties related to subsurface characteristics. The combination of different methods improve the accuracy and reliability of geometry definition and deposit material characterization. For a more detailed description of each geophysical method, please refer to the following report *D.T1.3.1: "Benchmark report on geophysics and non-intrusive investigation techniques for quantification of the potential resources located on a PMSD"*.



Figure 6 : Photographs of the different geophysical methods deployed on La Louvière site with A) EM, B) MAG, C) ERT/IP and SRT/MASW.

In duferco site, the following mapping methods were used:

- Electromagnetic induction (EMI) is used to map changes (generally at a few depth ranges) in electrical conductivity and magnetic susceptibility to reveal a different composition of the soil in terms of porosity, water saturation, clay and metal content ( Figure 6A).
- Magnetometry (MAG) maps changes in total magnetic field or vertical magnetic field gradient to identify areas containing objects disrupting locally the geomagnetic field ( Figure 6B).

More focused 2D/3D methods, providing detailed information about changes of physical properties with depth, were applied along distinct profiles (

Figure 6C). These methods include:

- Electrical Resistivity Tomography (ERT) aims to determine the electrical resistivity distribution of the subsoil. It can be used to discriminate different soil materials or investigate changes in water content.
- Induced Polarization (IP) is used in combination with ERT to quantify the chargeability distribution of the subsoil. Chargeability can highlight zones containing more electronic conductors (e.g., metallic scraps), areas with more organic matter or clayey formation.
- Seismic Refraction Tomography (SRT) and Multichannel Analysis of Surface Waves (MASW) aims to determine the seismic p-wave and surface wave velocities distributions. They can be used to characterize the stiffness structure of the subsurface indicating layers of different composition and the transition to the geological host.

In the next section, the equipment used and the acquisition parameters for each selected method are summarized.

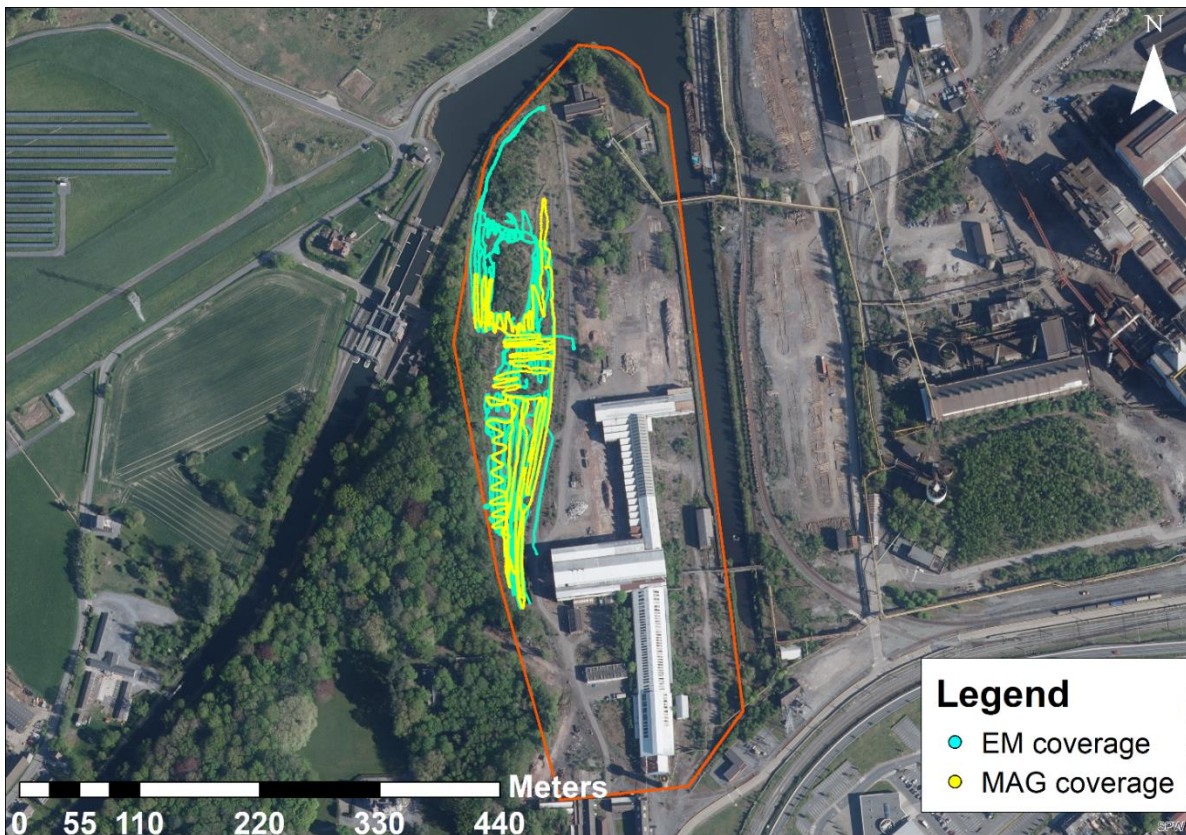


Figure 7 : EMI and MAG coverage on the old factory.

EMI data were acquired using a [Mini-explorer from GF Instruments](#). The Mini-explorer allows exploring simultaneously electrical properties of soil layers with a thickness of 0.5 m, 1 m and 1.8 m. Both quadrature (related to the electrical apparent conductivity) and in-phase (related to the apparent magnetic susceptibility) components were recorded. In addition, a GPS Trimble R10 (without RTK correction) was connected to the system for accurate positioning.

MAG data were acquired with a portable caesium magnetometer model [G-858 from Geometrics](#). All data were recorded in vertical gradient mode (which allow the deepest prospection) with 1 m separation between sensors and 0.6 m above ground level. For positioning, all data were continuously synchronized with a GPS Trimble R10 (without RTK correction).

As EMI and MAG are disrupted by human installations, they were only acquired in the western part of the old factory area. The area covered with the different devices is presented in Figure 7.

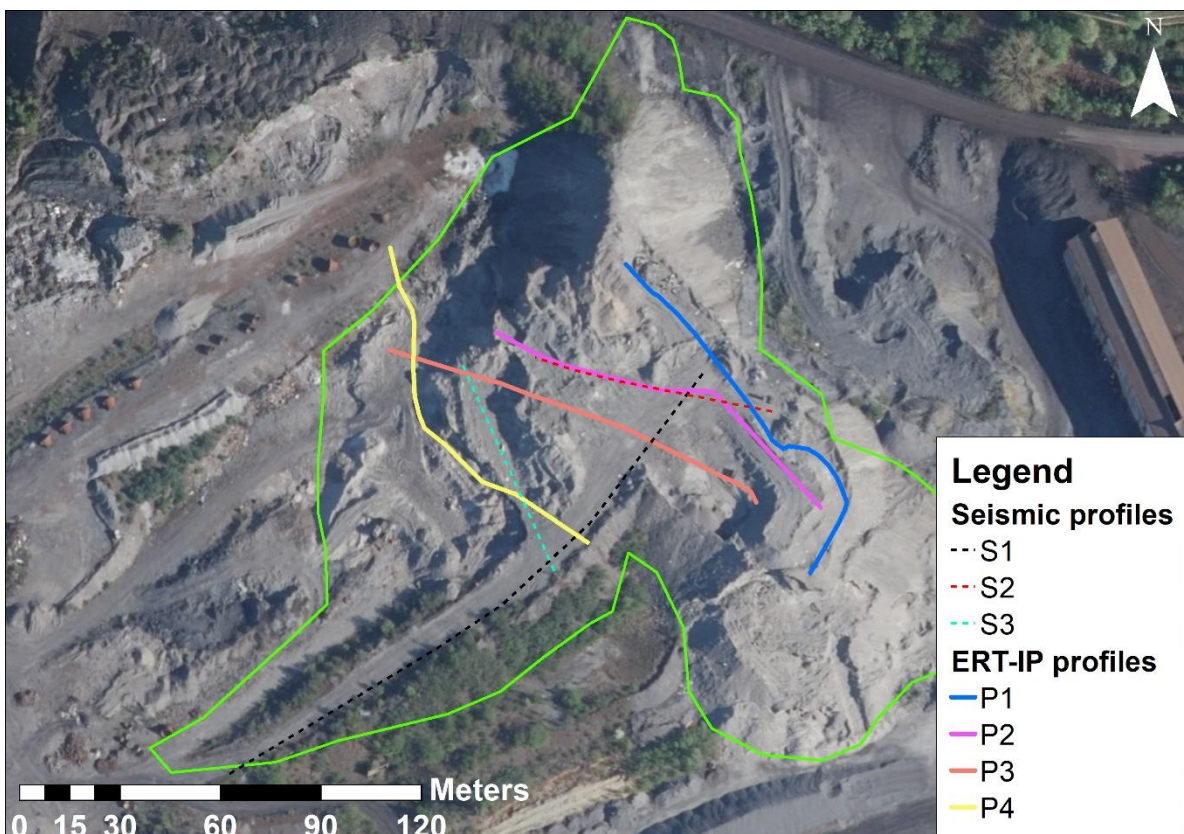


Figure 8 : Positioning of ERT-IP and seismic profiles on the white slag heap.

ERT and IP data were acquired with a [Terrameter LS system from ABEM](#). In the white slag heap, 4 2D profiles were deployed, each containing 64 stainless steel electrodes spaced by 2 m. To derive a 3D resistivity/chargeability model, data acquisition was carried out simultaneously on two profiles (respectively P1-P2, P2-P3, P3-4) so that not only inline but also crossline measurements were collected. Given the steep topography on the sides of the white slag heap and the uneven terrain on its top, it was not possible to setup straight or parallel profiles (see Figure 8). For the data acquisition, a gradient array with a 's' factor equals to 7 was used (Dahlin and Zhou 2006). It was complemented with bipole-bipole acquisition. Electrical current was injected for 2 s (delay of 0.8 s and acquisition of 1.2 s) and the voltage decay was measured during 1.86 s after the current was switched off. Measurements were repeated twice to estimate the repetition error and to improve signal quality. A sample of reciprocal measurements was also collected for each profile to assess the quality of data. A fifth profile was also deployed in the old factory area with 64 electrodes spaced by 1 m (see Figure 9). The same acquisition settings were applied (except that the bipole-bipole data were not collected).

Three SRT and MASW profiles were deployed in the white slag heap (see dashed lines in Figure 8). The data were acquired using a DAQlink 4 system and a fixed receiver array of 48 vertical geophones (4.5 Hz natural frequency). Roll along acquisition was used to move the receiver array in order to cover the whole survey area. The first profile (P1) contained 96 geophones spaced by 2 m, the second profile (P2) contained 73 geophones spaced by 1 m, and the last profile (P3) contained 46 geophones spaced by 1.5 m. A 5 kg sledgehammer was used as a source together with a ground-coupled nylon plate. The receiver array was kept fixed and the source was moved every four geophones from one end of the spread. In order to increase the signal to noise ratio, a total of 10 shots were stacked at each shot location.

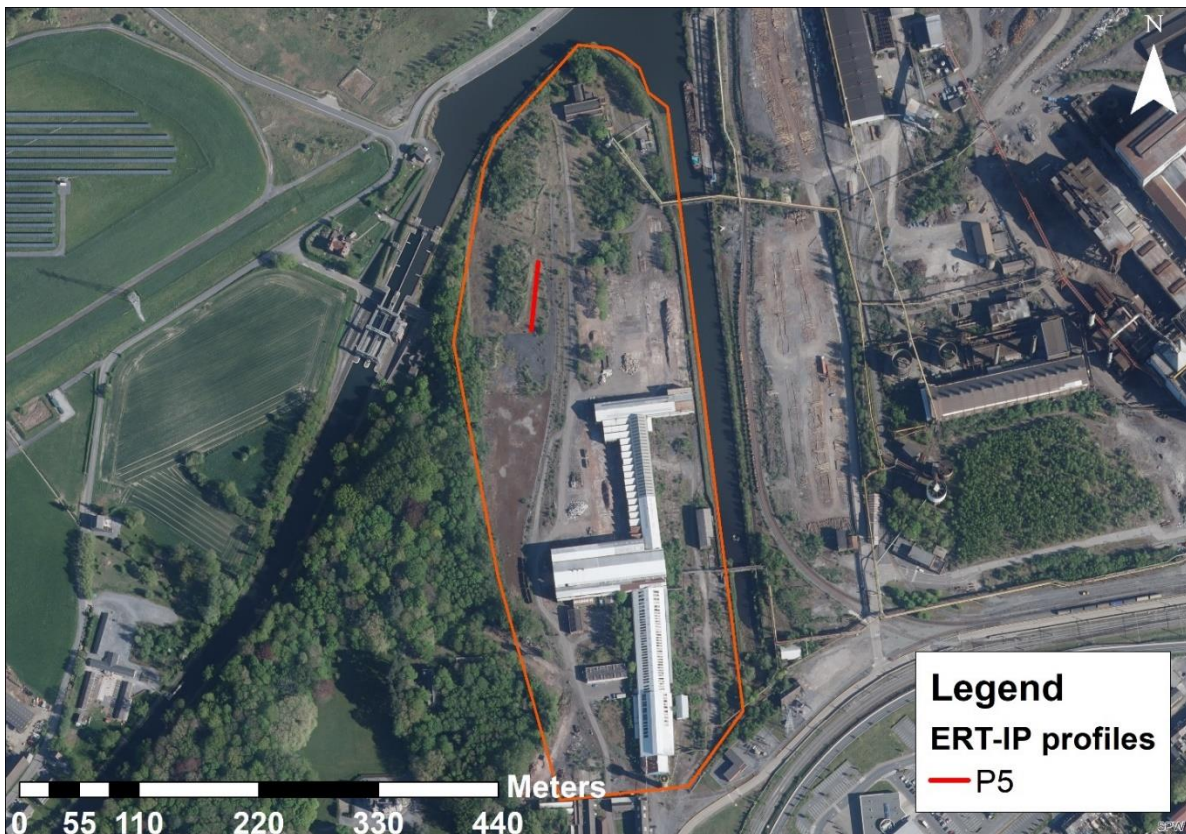


Figure 9 : Location of the fifth ERT-IP profile in the old factory area.

## 2.2 GEOPHYSICAL PROCESSING AND RESULTS

The processing of data and results of each geophysical method are described in the following section.

### 2.2.1 EMI results

The results of the EMI measurements are presented in the form of maps in Figure 10. These maps show the apparent electrical conductivity, ECa (A, C, E) and the apparent magnetic susceptibility, MSa (B, D, F) at three different depths below the surface corresponding to the depths of maximum sensitivity of the EMI coil configuration. Note that only the positive values of the ECa are displayed on the maps. The very high electrical conductivities observed in the southern part of the study area suggest that the assumption of a low induction number is probably not verified, so that the ECa and MSa values displayed should be interpreted with caution. Although the different maps cannot be interpreted quantitatively, they nevertheless provide useful information. A clear distinction can be made between the southern and northern parts of the area investigated. The former exhibits much higher ECa and MSa values which tends to suggest a higher metal content. The difference in soil

type was also visible on site, with the southern part being free of vegetation and having much harder surface than the northern one.

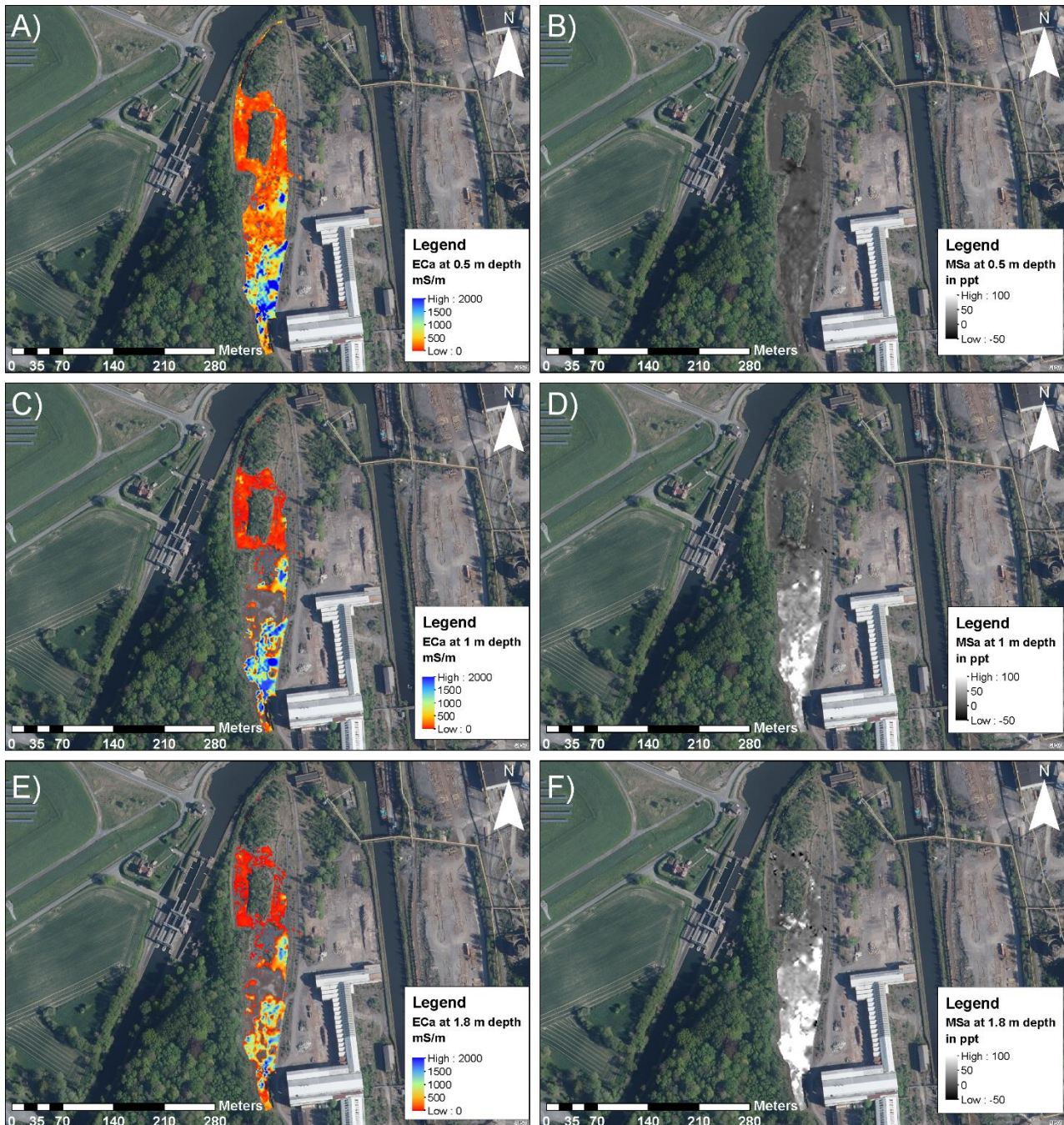


Figure 10 : EMI results with apparent electrical conductivities ECa (A, C, E) and apparent magnetic susceptibility MSa (B, D, F).

## 2.2.2 MAG results

After processing, MAG data appears to be of poor quality. Indeed, the magnetic field in many locations exceeded the range of magnetic field values allowed by the sensors (see the coverage map with good data points in green in Figure 11). Although disappointing, the results nevertheless confirm the interpretation of EMI data suggesting a higher metal content in the southern part where most of the MAG data could not be measured due to too high magnetic field values. Note the expected total magnetic field amplitude provided by the World Magnetic Model in the vicinity of the site is 48 793.5 nT.

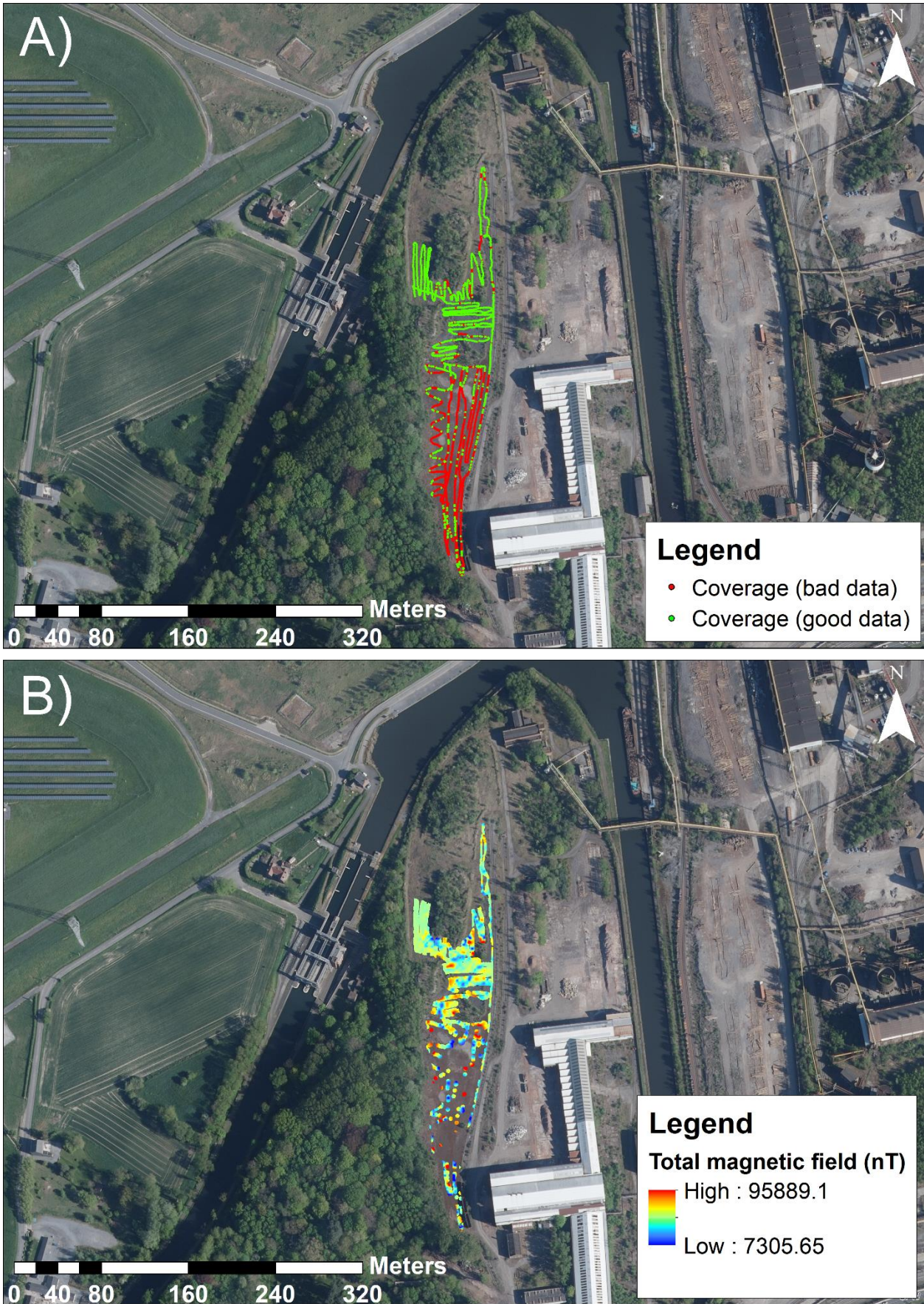


Figure 11 : Results of the magnetic survey with A) good (green) and bad (red) data, B) total magnetic field amplitude.

## 2.2.3 ERT and IP results

Data collected were first filtered by removing all measurements characterized by a repetition error on the measured resistance greater than 5%. Then, in order to weight the data in the inversion process, an error model was calculated on the resistance value using the reciprocal data collected during the acquisition (see Figure 12). The absolute error is 2.89E-2 Ohm and the relative error 2.27 %.

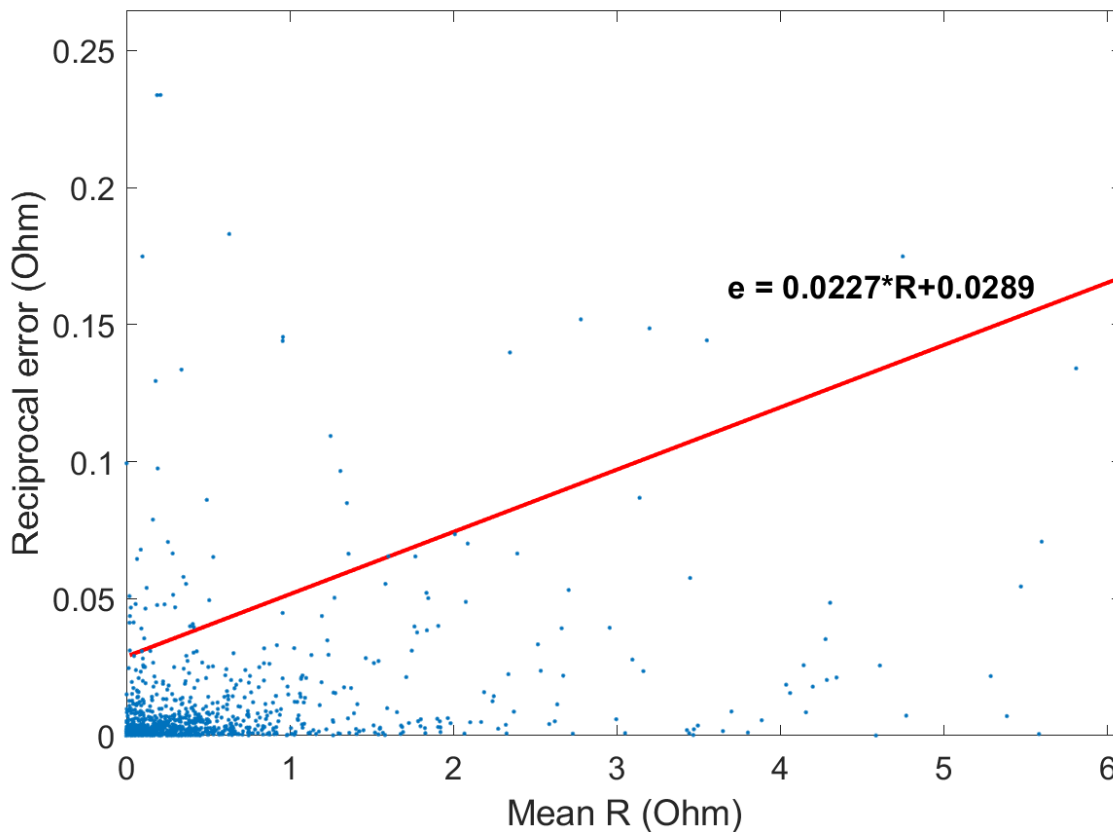


Figure 12 : Error model on the measured electrical resistance data estimated on the basis of reciprocal data.

The weighted data were inverted with BERT (Günther et al. 2006) using a robust constraint on the data and a blocky constraint on the model. The 3D models obtained with BERT satisfies the error weighted chi-square,  $\chi^2 = 1$  meaning that the data are fitted to their error level. Figure 13 shows the final 3D resistivity and chargeability models together with the electrodes position. Note that all coordinates are expressed in Belgian Lambert 1972.

Figure 13 reveals contrasted electrical signatures depending on the location in the models. Electrical resistivity is generally low although big patches of with large values are also observed in some places. The chargeability model is more heterogeneous. The very larges values observed at the surface of the model corresponds to the area of the heap known as “tout-venant”, meaning that it contains a bit of everything and in particular quite a lot of metallic objects/scraps.

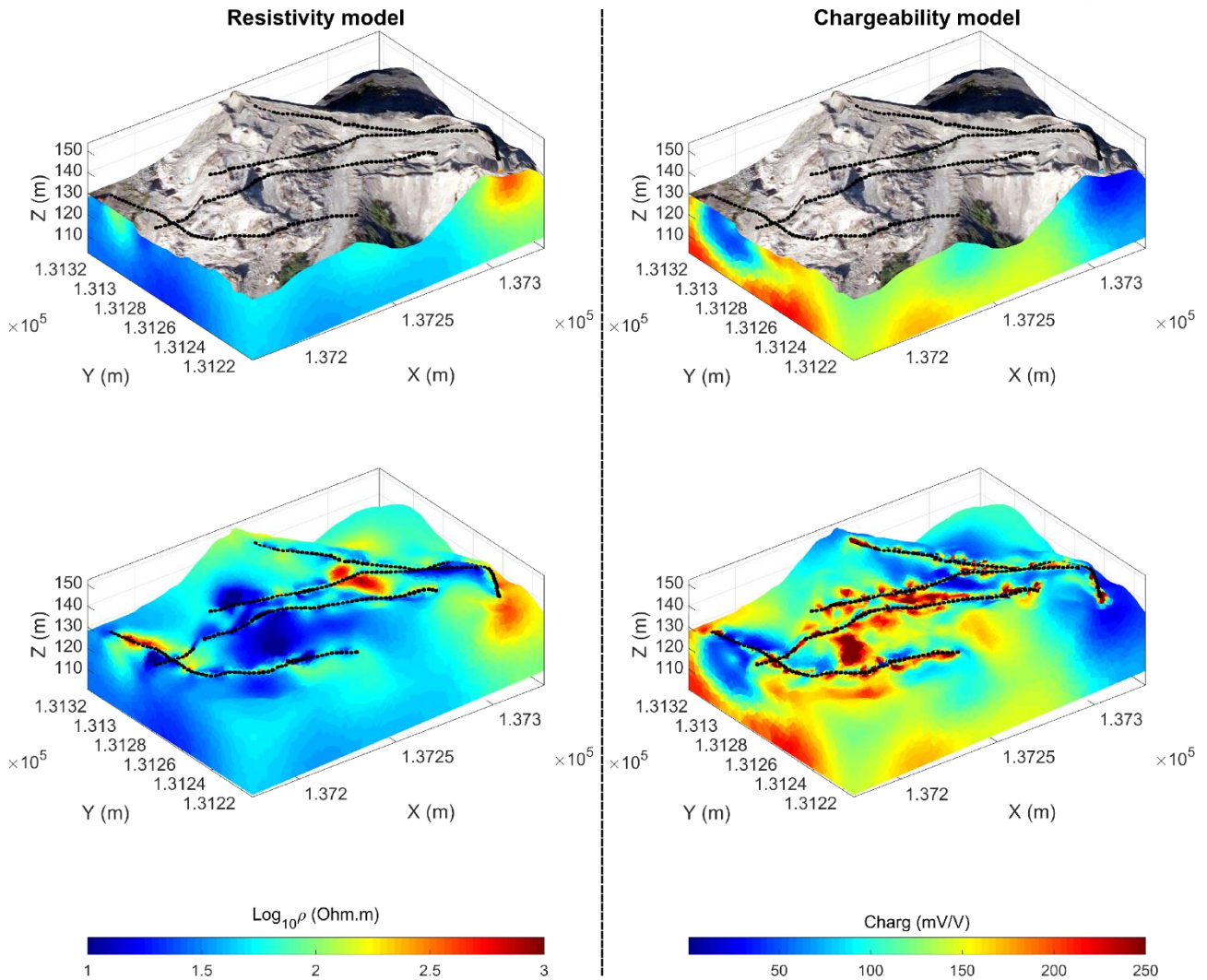


Figure 13 : 3D electrical resistivity (left) and chargeability (right) models with (top) and without (bottom) satellite image draping. The electrodes are represented by the black dots.

To further investigate the electrical properties at depth, the models are first clipped at an altitude of 138 m (above mean sea level). The resulting clipped model is shown in Figure 14. The large resistive anomaly found in Figure 13 is also present at depth in Figure 14 A. It is furthermore characterized by low chargeability which gives an indication on the nature of the material of which it is composed, probably demolition waste or refractory materials. This anomaly separates two large anomalies of high chargeabilities. The one to the west (in the center of Figure 14 B) corresponds to the “Tout-venant” area already visible in Figure 13 B. The one to the east (right-hand side of Figure 14 B) is characterized by even higher chargeabilities and may correspond to a zone of more metal-rich slag.

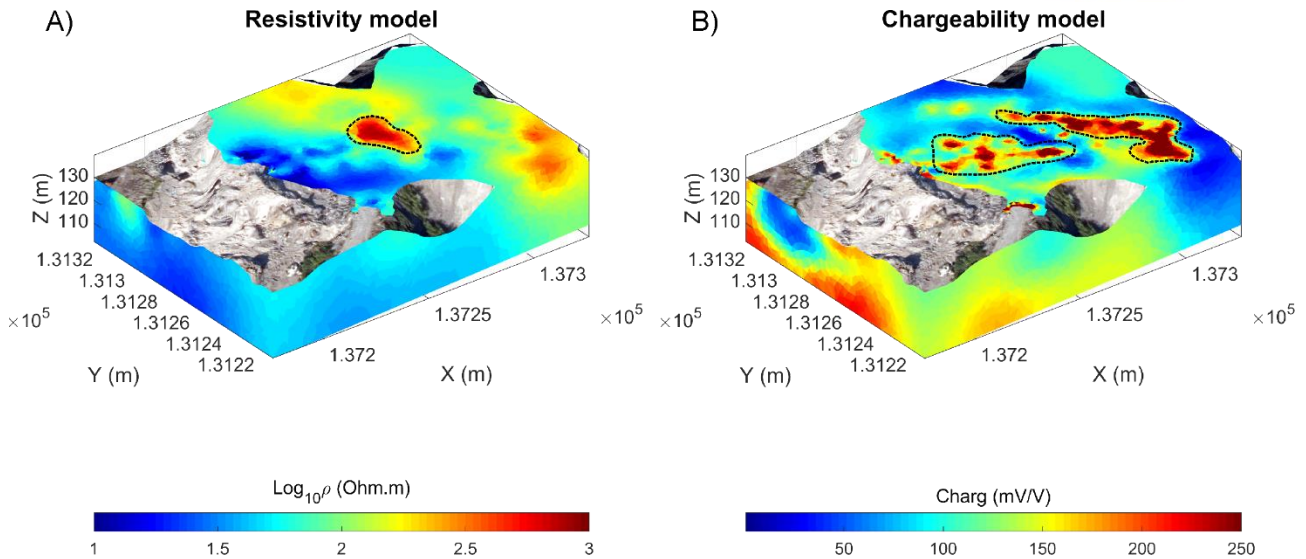


Figure 14 : Clipping of 3D resistivity (A) and chargeability (B) models at an elevation of 138 m.

Figure 15 gives an idea of the vertical extent of the features identified above. Note that the lower part of the chargeability model (see Figure 15 B and E) shows very high values, which is rather unlikely given the expected presence of alluvial deposits at that level (as revealed by old topographic maps from the 19th century). It is therefore likely that what is observed on the chargeability model is an artefact arising from a lower sensitivity of the model parameters (see Figure 15 C and F).

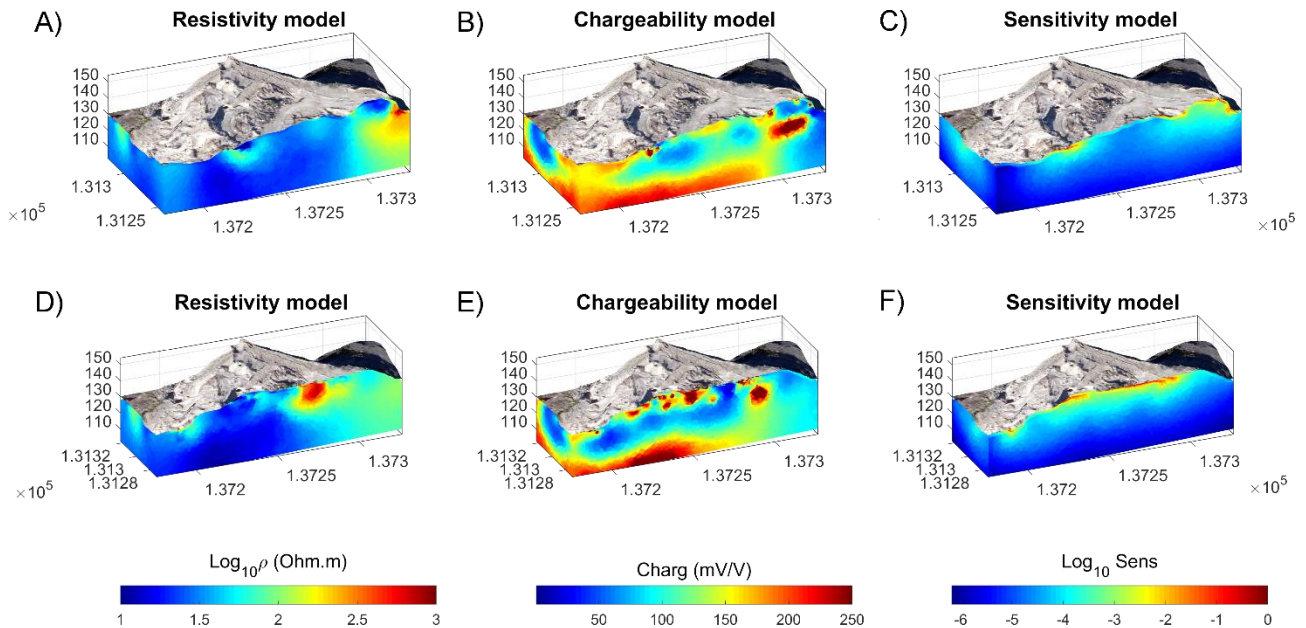


Figure 15 : Clipping of 3D resistivity (A, C) and chargeability (B, D) models at the northern coordinates 131240 m (A and B) and 131270 m (C and D).

Figure 16 shows the electrical resistivity and chargeability models obtained in P5 together with the associated normalized model sensitivity. The results are difficult to interpret as the soil was probably highly disturbed over the years as revealed by the heterogeneous patterns visible in Figure 16. A thin layer at the soil surface (approximately 1.5 m thick) exhibits higher chargeability probably due to the presence of small metallic objects/scraps. Chargeability anomalies at depth indicate potentially the presence of slags or large metallic pieces. The more resistive anomalies (generally also characterized by low chargeability) may reveal construction/demolition waste or refractories.

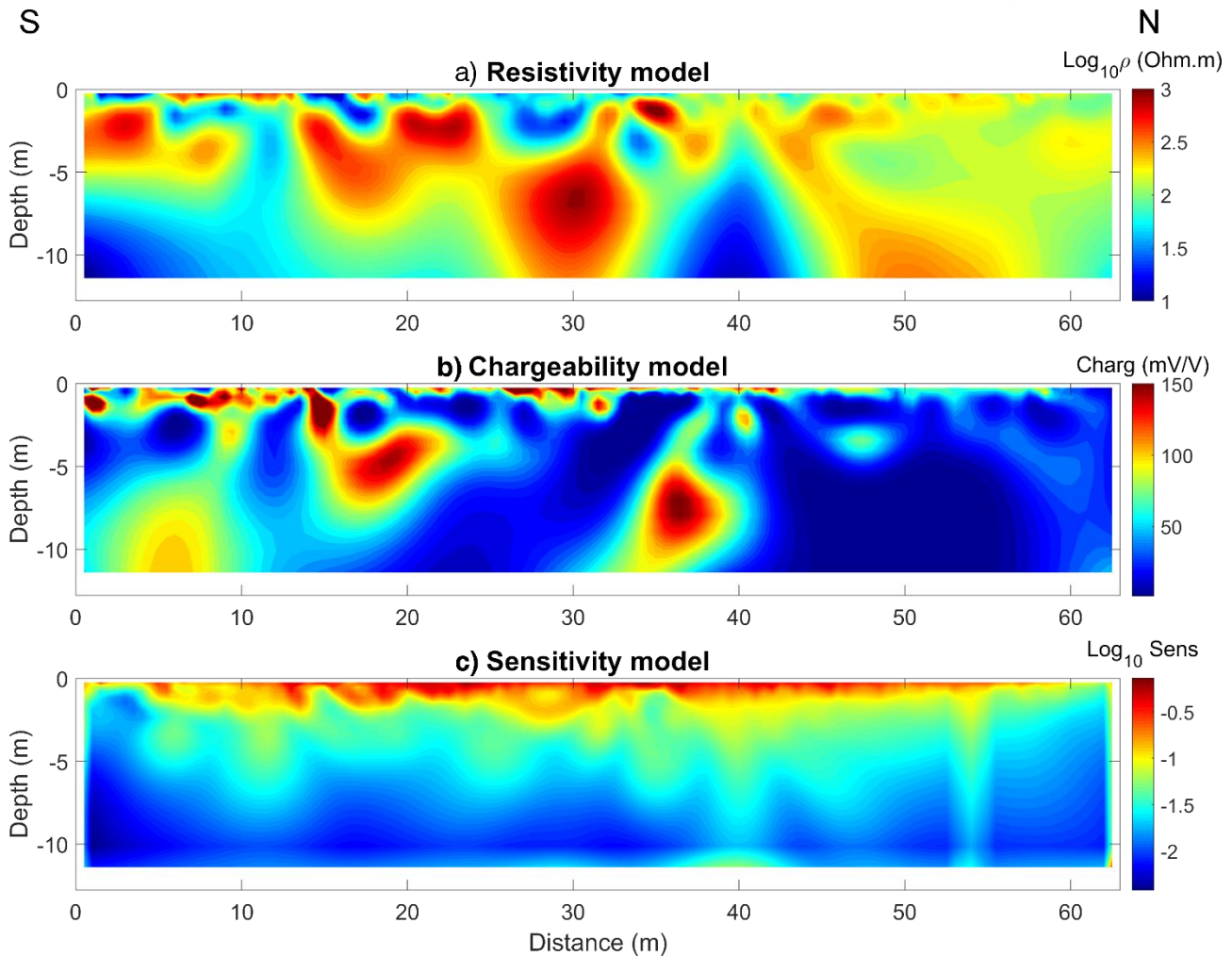


Figure 16 : Electrical resistivity (a), chargeability (b) and sensitivity (c) models obtained in P5.

## 2.2.4 SRT – MASW results

The picking of first arrival of p-waves was carried out with the software SARDINE developed by the team of University of Liège. The SRT inversion was then carried out with the open source library of pyGIMLi (Rücker et al. 2017).

The software SurfSeis6 (Kansas Geological Survey KGS) was used to process the surface wave data. Each shot record was transformed to calculate the phase velocity-frequency distribution, also known as the dispersion curve, and the fundamental mode of each dispersion curve was then picked. Finally, the dispersion curves were inverted from each profile to derive the 2D shear-wave velocity models.

Globally, the seismic data were of poor quality which can be explained by several factors. First, the ambient noise on the site was high due to the ongoing demolition of the facilities nearby. Second, the top layer appears to be very hard (probably due to compaction and chemical reactions occurring between the highly reactive slags and rain water). The presence of such a layer tends to mask the underlying layers, which greatly limits the depth of investigation. Third, the presence of buried scatterers also probably contributed to the poor quality of seismic data. To illustrate this, the results of SRT inversion are presented in Figure 17 where the areas with poor data coverage are blanked. As shown, the information provided by SRT is very limited only revealing a few interfaces at shallow depth as in S1 or S3. MASW results are not shown because the error associated to the model parameters is too high.

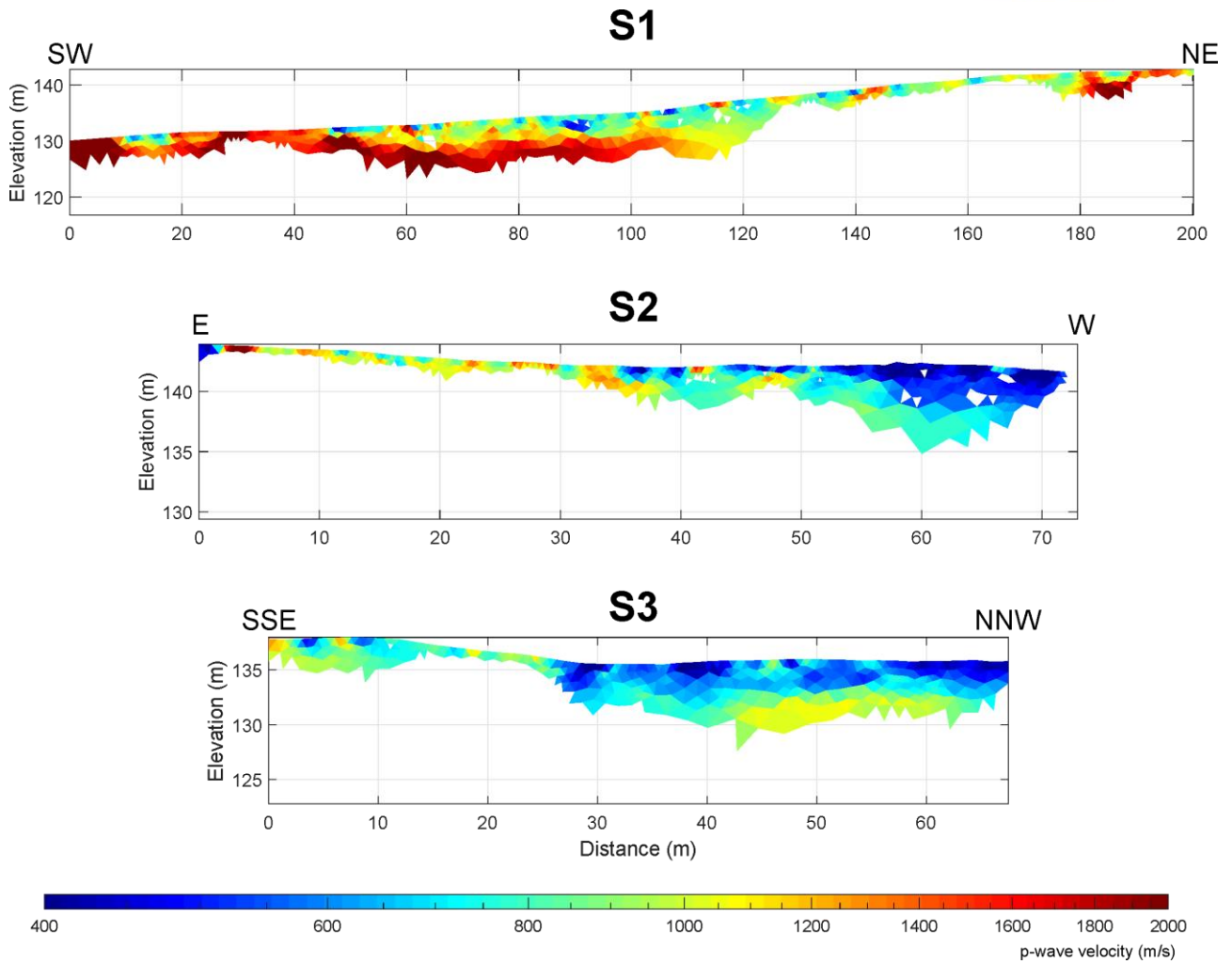


Figure 17 : p-waves velocity models obtained in S1, S2 and S3. Only the areas with sufficient data coverage are displayed.

## 3 CONCLUSION

---

Several geophysical methods were applied on the Duferco - La Louviere site. Two areas were investigated within the framework of the project: the white slag heap and the old factory. Among the methods tested, electrical resistivity tomography and induced polarization offered the most promising results with contrasting electrical signatures that could be related to areas of different metal content. High chargeability and low resistivity are considered as a good indicator for detecting potentially interesting areas for materials valorization. Where it is not possible to implement electrical profiles, electromagnetic induction can still offer valuable information to detect such areas although the resolution with depth of the method is more limited. In such situations, low electrical conductivity and high magnetic susceptibility are thought to indicate the most interesting areas. These assumptions need however to be validated with ground truth data consisting of soil samples collected at the locations targeted by geophysics and analyzed in laboratory for their content in major elements. Details of the sampling plan proposed after the geophysical survey can be found in *DI3.1.2: Site specific investigation plan and schedule*. The results of the correlation between the geophysical results and the chemical analyses of the samples can be found in *DI3.2.3: Correlation report of characterization studies based on information from geophysical investigations and traditional investigations*.

## 4 REFERENCES

---

Dahlin, T. and Zhou, B. (2006) Multiple-gradient array measurements for multichannel 2D resistivity imaging. *Near Surface Geophysics* 4(2), 113-123.

Günther, T., Rücker, C. and Spitzer, K. (2006) Three-dimensional modelling and inversion of DC resistivity data incorporating topography—II. Inversion. *Geophysical Journal International* 166(2), 506-517.

Rücker, C., Günther, T. and Wagner, F.M. (2017) pyGIMLi: An open-source library for modelling and inversion in geophysics. *Computers & Geosciences* 109, 106-123.